Split exponential track length estimator for Monte-Carlo simulations of small-animal radiation therapy

2014 Phys. Med. Biol. 59 7703

(http://iopscience.iop.org/0031-9155/59/24/7703)

IOP Publishing | Institute of Physics and Engineering in Medicine Physics in Medicine & Biology

Phys. Med. Biol. **59** (2014) 7703–7715 doi:10.1088/0031-9155/59/24/7703

Split exponential track length estimator for Monte-Carlo simulations of small-animal radiation therapy

F Smekens[1], J M Létang[1], C Noblet[2], S Chiavassa[2,3], G Delpon[2,3], N Freud[1] S Rit[1] and D Sarrut[1]

[1] Université de Lyon, CREATIS CNRS UMR5220, Inserm U1044, INSA-Lyon, Université Lyon 1, Centre Léon Bérard, France
[2] Inserm UMR 892, IRT UN, F-44007 Nantes, France
[3] Institut de Cancérologie de l'Ouest, Centre René Gauducheau, Saint-Herblain, France

E-mail: francois.smekens@creatis.insa-lyon.fr

Received 4 August 2014, revised 2 October 2014
Accepted for publication 20 October 2014
Published 24 November 2014

Abstract

We propose the split exponential track length estimator (seTLE), a new kerma-based method combining the exponential variant of the TLE and a splitting strategy to speed up Monte Carlo (MC) dose computation for low energy photon beams. The splitting strategy is applied to both the primary and the secondary emitted photons, triggered by either the MC events generator for primaries or the photon interactions generator for secondaries. Split photons are replaced by virtual particles for fast dose calculation using the exponential TLE. Virtual particles are propagated by ray-tracing in voxelized volumes and by conventional MC navigation elsewhere. Hence, the contribution of volumes such as collimators, treatment couch and holding devices can be taken into account in the dose calculation.

We evaluated and analysed the seTLE method for two realistic small animal radiotherapy treatment plans. The effect of the kerma approximation, i.e. the complete deactivation of electron transport, was investigated. The efficiency of seTLE against splitting multiplicities was also studied. A benchmark with analog MC and TLE was carried out in terms of dose convergence and efficiency.

The results showed that the deactivation of electrons impacts the dose at the water/bone interface in high dose regions. The maximum and mean dose differences normalized to the dose at the isocenter were, respectively of 14% and 2% . Optimal splitting multiplicities were found to be around 300. In all situations, discrepancies in integral dose were below 0.5% and 99.8% of

the voxels fulfilled a 1%/0.3 mm gamma index criterion. Efficiency gains of seTLE varied from 3.2×10^5 to 7.7×10^5 compared to analog MC and from 13 to 15 compared to conventional TLE.

In conclusion, seTLE provides results similar to the TLE while increasing the efficiency by a factor between 13 and 15, which makes it particularly well-suited to typical small animal radiation therapy applications.

Keywords: variance reduction, track length estimator, Monte Carlo simulation, small animal radiotherapy, seTLE

(Some figures may appear in colour only in the online journal)

1. Introduction

For realistic dosimetric applications, Monte Carlo (MC) simulations are known to be precise and generic but very time consuming methods. Most of the recent developments propose variance reduction techniques (VRTs) in order to improve MC efficiency. A large number of VRTs, such as the Russian roulette, particle splitting and range/energy cut, have been investigated for high energy photon beam applications. It has been shown that particle splitting gives a relatively large efficiency gain (factor 5–9), followed by the optimized particle transportation (factor 1.6 to 2.4) (Kawrakow and Fippel 2000). Indeed, a significant time can be wasted in tracking useless particles or in accounting for low probability physical processes.

The splitting strategy, consisting of the replication of particles undergoing a physical process, was successfully applied in many situations (Brualla *et al* 2009, Grevillot *et al* 2011, Rodriguez *et al* 2012), mainly for handling the bremsstrahlung effect involved in x-ray production. The use of this strategy, sometimes combined with the Russian roulette, is now commonly available in the majority of MC platforms. On the other hand, the optimization of particle transport regroups several MC parameters (i.e. energy cut-offs and maximum step sizes for electrons and energy cuts and kerma approximation for photons). The highest gains are provided by the electron cut-off energy and kerma approximation (Kawrakow and Fippel 2000).

During the last decade, small animal radiotherapy has become an efficient modality for preclinical studies (Verhaegen *et al* 2011). As the precision of devices increases, the MC methods were found to be well adapted to take into account low energy photon beams (below 250 keV), small beam sizes (from 20 to 1 millimeter) and high resolution volumes (typical voxel size about 0.2 mm). Although this modality could benefit from recent MC improvements, VRTs had to be adapted to the low energy domain. Several papers recently proposed optimal splitting settings for low energy photon production and dosimetry (Mainegra-Hing and Kawrakow 2006, Bazalova *et al* 2009). The use of an analytical source model in order to replace the simulation of x-ray production was also proposed (Granton and Verhaegen 2013). Given the low amount and energy of produced electrons, the kerma methods, based on a complete deactivation of electron transport, seem well adapted to improve the speed of the particle transport.

In 1987, Williamson proposed several kerma estimation methods in order to speed up MC simulations (Williamson 1987). The most promising techniques were the linear and exponential track length estimators (TLE and expTLE). Nowadays, the TLE method is the state-of-the-art VRT for low energy applications, providing acceleration factors of about two orders of magnitude compared to analog MC (Mittone *et al* 2013, Baldacci *et al* 2014). To our knowledge, the expTLE was not applied in its original form and is not available in MC codes.

In 2009, we proposed a new kerma-based method mixing MC splitting, ray casting and expTLE dose scoring (Smekens *et al* 2009). We showed that this approach could provide an additional efficiency gain of about one order of magnitude compared to TLE for a typical synchrotron radiation treatment plan. However, the method detailed in this article was merely a proof-of-concept and had several shortcomings (ideal photon source, no beam modifiers), preventing its use for realistic dosimetric applications.

In this paper, we revisit the split exponential track length estimator (seTLE) in light of its application to dose simulation in small animal radiotherapy. First, the concept of multiplicity (splitting number) is extended to the primary photon source in order to take into account any source configuration. Then, the genericity of the method is improved with a new virtual particle used to perform the navigation in volumes surrounding the voxelized geometry (collimators, treatment couch, etc.). The seTLE was developed within the GATE/Geant4 MC framework (Jan *et al* 2011, Sarrut *et al* 2014). Originally dedicated to PET imaging simulations, GATE is an open source code which proposes now a complete set of scoring methods for imaging and radiotherapy issues, including the conventional TLE method.

2. The split exponential track length estimator

The seTLE combines three concepts described in this section: MC splitting, hybrid navigation and expTLE dose calculation. The global organisation of the method is the following. For any new photon or modification of the characteristics of an existing one, the splitting procedure is applied. Then, the split photons are transformed into virtual particles and tracked using the hybrid navigation. Only these virtual particles are used to calculate the dose distribution.

2.1. Splitting strategy

Classical MC splitting consists in adding M photons, M being the splitting multiplicity, in the simulation with a $1/M$ weight when a particular interaction occurs. The characteristics of the new photons are generally generated using the MC engine.

In the seTLE method, this concept, previously applied to physical processes only (Smekens *et al* 2009), is extended to the history of all photons in the simulation. This includes physical interactions (Compton and Rayleigh scattering and fluorescence) and new primary photons. This approach takes into account the characteristics of any source (energy, direction and spatial distributions) as well as any physical interaction model included in GATE/Geant4 (standard, Livermore, Penelope, etc.). In practice, each incident photon and interaction site respectively produce M_{p} and M_{s} additional particles (primary and secondary multiplicities) by using the primary event and the interaction random generator. Then, instead of propagating the split photons like conventional MC particles, a hybrid navigation combining MC and ray casting is used.

2.2. Hybrid navigation

Previously, a ray casting technique optimized for voxelized geometries was used to propagate split particles (Freud *et al* 2008). However, this approach does not handle non-voxelized volumes introduced in the MC scene in many realistic simulations (treatment couch, collimators, etc.).

In order to fully integrate the seTLE in GATE/Geant4, a hybrid navigation system is introduced. The aim of this navigation system is to support the dose calculation by propagating

the split photons according to the expTLE dose calculation requirements (section 2.3) as efficiently as possible. This is achieved by replacing the split photons with hybrid particles called 'hybridinos'. Having no physical processes, the hybridinos propagate the photon characteristics through any MC volume in a straight line. In order to keep the advantages of both ray casting and MC navigation systems, hybridinos are propagated using optimized ray casting inside the voxelized geometry and using generic MC navigation outside.

2.3. Dose calculation: linear and exponential track length estimators

The TLE and expTLE dose calculation methods implemented in GATE/Geant4 were originally defined by Williamson (1987). In the TLE approach, the dose is calculated during photon transportation between production/interaction sites. For each step that occurs in voxel i along the photon path, the dose is expressed as follows:

$$D_i^{\mathrm{TLE}} = \frac{E \times \mu_{\mathrm{en}}(E, m_i) \times L_i}{\rho_i \times V} \tag{1}$$

where D_i^{TLE} is the dose deposited in voxel i of volume V and density ρ_i, $\mu_{\mathrm{en}}(E, m_i)$ is the energy absorption coefficient for photon energy E in material m_i and L_i is the step length of the photon in the voxel. In the expTLE method, both attenuation and energy absorption are calculated in a single step. For each step, the weight of the photon is updated using the Beer–Lambert law:

$$w_i^{\mathrm{out}} = w_i^{\mathrm{in}} \times \exp[-\mu(E, m_i) \times L_i] \tag{2}$$

where w_i^{in} and w_i^{out} are the entrance and exit weights for the step of length L_i in material m_i and $\mu(E, m_i)$ is the attenuation coefficient of this material for the photon energy E. Then, the dose is calculated as follows (Smekens *et al* 2009):

$$D_i^{\mathrm{expTLE}} = \frac{E \times \mu_{\mathrm{en}}(E, m_i) \times [w_i^{\mathrm{in}} - w_i^{\mathrm{out}}]}{\rho_i \times V \times \mu(E, m_i)} \tag{3}$$

where D_i^{expTLE} is the dose deposited in the current voxel. It is worthy of note that if $\mu(E, m_i) \times L_i \ll 1$, we have the following relationship between the scoring methods:

$$D_i^{\mathrm{expTLE}} = w_i^{\mathrm{in}} D_i^{\mathrm{TLE}} \tag{4}$$

The main difference between the TLE and expTLE methods relies in the fact that the expTLE replaces a stochastic decision (absorption or scattering of the photon) by its expected outcome characterized by the attenuation coefficient $\mu(E, m)$. In order to avoid any bias, the dose calculation must be performed from the production/interaction site of the photon to the exit of the MC scene. This requires the use of a specific navigation system dedicated to the dose calculation (section 2.2) in addition to the classical MC photon tracking system.

3. Monte Carlo simulations

3.1. Small animal test cases and micro-irradiator setup

Simulations were performed for two realistic small animal treatment plans delivered by the micro-irradiator X-RAD 225 Cx (Clarkson *et al* 2011). The first plan was the irradiation of a mouse bronchus (figure 1, left) and the second plan was the irradiation of the femoral head of a rat (figure 1, right). The treatment plan was the same for both volumes: a 360° arc irradiation with a beam angle spacing of 5°. Collimators of 5 mm and 2.5 mm diameters were modeled

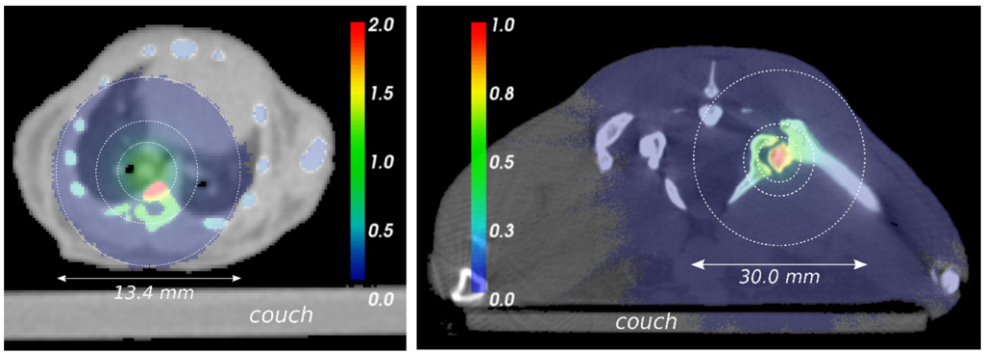

Figure 1. Dose distributions for mouse (left) and rat (right) treatment plans normalised by the dose at the isocenter. For splitting multiplicity, efficiency and dose comparisons, three spherical ROIs (dashed white lines) were defined for each test case.

for the rat and mouse volumes respectively. Cone-beam CT acquisitions were segmented in 5 materials: air, carbon (for the treatment couch), soft tissue, lung tissue and cortical bone (ICRU-44 elemental compositions). The volume dimensions were $50.8 \times 35.0 \times 30.0$ mm^3 (mouse) and $94.2 \times 52.6 \times 26.8$ mm^3 (rat) for a voxel size of $0.2 \times 0.2 \times 0.2$ mm^3 in both cases.

The MC photon source was the analytical source model recently proposed for this device (Granton and Verhaegen 2013). For all field sizes, the measured fluence image of the focal spot was used as a photon source. The photon energies were stochastically sampled in a 225 kVp spectrum of 1 keV resolution generated using the SpekCalc program (Poludniowski *et al* 2009). As reported by Granton *et al*, the photon transmission through the brass insert of the collimator can reach 13% whereas the transmission through the lead insert can be neglected. In order to take into account the transmission through brass without wasting time simulating photon interactions in lead, the photon directions were focused using a virtual collimator system. This collimator consisted in a virtual surface matching perfectly the physical circular collimator aperture plus 1 mm margin. In all situations, no phase space file was used.

3.2. Kerma approximation and electron production cuts

The main approximation in kerma-based methods is the deactivation of electron transportation and the local absorption of the electron kinetic energy. The physical processes are therefore restricted to photoelectric effect, Compton and Rayleigh scattering and fluorescence. However, to our knowledge, the consequence of this approximation has not been evaluated for small animal radiotherapy.

To quantitatively estimate the accuracy loss due to the absence of electron tracking, we performed a complete analog MC simulation with the tracking of electrons in the two typical irradiation cases. We used the *emlivermore* physics list provided by GATE/Geant4. This physics list contains a complete description and setup of electromagnetic processes. For this particular test, the dose distributions obtained with an electron production cut, i.e. the minimal CSDA range for the electron to be produced, of 10 μm and 1 m were compared. An electron production cut of 1 m, which corresponds to an energy threshold in air higher than the maximal incident photon energy (380 keV versus 225 keV), is sufficient to deactivate all electrons productions in the simulation. In other simulations (sections 3.3 and 3.4), we assumed the deactivation of electron transport with an electron production cut of 1 m.

3.3. Multiplicity: sensitivity study

For VRTs based on the splitting approach, the value of the splitting multiplicity influences the efficiency of the simulation. In the seTLE method, the primary and secondary multiplicities have to be correctly set to obtain the highest efficiency. However, the optimal values of the multiplicities depend on the local ratio between primary and secondary dose contributions, e.g. a large primary dose contribution entails a primary optimal multiplicity M_p reduced with respect to the secondary one M_s.

In order to better quantify the separate influence of the primary multiplicity M_p and the secondary multiplicity M_s on the simulation efficiency, we performed for each test case two independent series of simulations. The series for the primary multiplicity was composed of 10 simulations with multiplicity values M_p varying from 1 to 1000 ($M_s = 0$) and the series for the secondary multiplicity was composed of 15 simulations with multiplicity values M_s varying from 1 to 800 ($M_p = 0$). For each simulation, the number of incident photons was fixed to 10^5. Finally, for each series of simulations, we represented the mean efficiency as a function of the multiplicity for the regions of interest (ROIs) R_1, R_2 and R_3 defined in the next section.

3.4. Dose and efficiency comparison

The two small animal treatment plans obtained with the seTLE dose scoring method were compared to their equivalents obtained with the analog MC and TLE methods without MC splitting VRT. All criteria described in this section were applied to the three ROIs for each small animal volume. These regions, presented in figure 1, consist in spherical layers of increasing diameters centered at the isocenter (4 mm, 7.2 mm and 13.4 mm for the mouse volume and 7.2 mm, 12 mm and 30 mm for rat volume). The small, medium and large ROIs were denoted R_1, R_2 and R_3 for the two test cases in the following. This choice was motivated by the high level of density heterogeneity in small animal models which complicates the use of classical percentages of the dose at isocenter.

First, the analog MC and seTLE methods were compared in terms of dose. A global dose comparison was performed by calculating the integral dose deposited in the ROI ($R_1 + R_2 + R_3$) and a local dose comparison was performed by using a gamma index test. The distance criterion was set to 0.3 mm and the dose criterion was 1% of the dose deposited in the voxel containing the isocenter for the analog MC method.

Second, the analog MC, TLE and seTLE methods were compared in terms of simulation efficiency. Global and local efficiencies were evaluated by calculating the mean efficiency in regions R_1, R_2 and R_3 and the voxel-by-voxel efficiency. The efficiency ϵ_k in the voxel k is calculated as follows:

$$\epsilon_k = \frac{1}{t \times \sigma_{\overline{d_k}^2}} \tag{5}$$

where t is the total simulation time obtained using a single CPU core (Intel® Xeon(R) CPU E5-1660, 3.30 GHz) and $\sigma_{\overline{d_k}}$ is the statistical uncertainty in dose in voxel k calculated using the history-by-history method described by Chetty *et al* (2006):

$$\sigma_{\overline{d_k}} = \sqrt{\frac{1}{N-1}\left(\frac{\sum_{i=0}^{N} d_{k,i^2}}{N} - \left(\frac{\sum_{i=0}^{N} d_{k,i}}{N}\right)^2\right)} \tag{6}$$

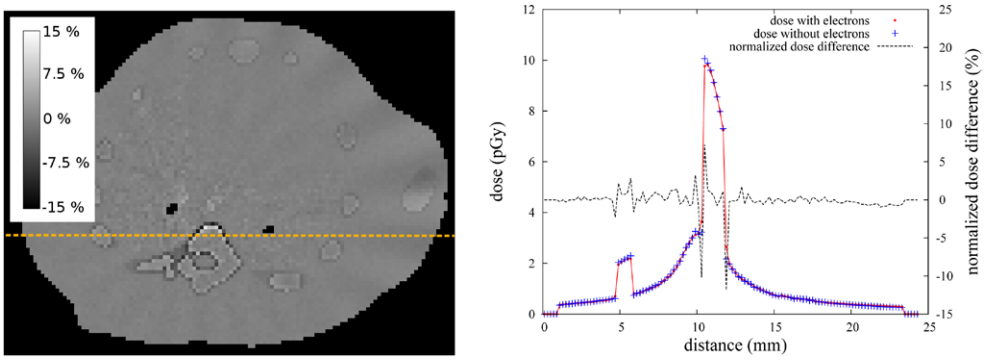

Figure 2. Dose difference normalized by the dose at isocenter $\frac{d_{10\mu m} - d_{1m}}{d_{10\mu m,(\mathrm{iso})}}$ (left) and dose profiles (right) for dose distributions with electron production cuts of 10 μm and 1.0 m obtained with the analog MC dose scoring.

where $d_{k,\,i}$ is the dose deposited in voxel k by an independent history i and N is the total number of incident photons. For the three dose scoring methods, the number of incident photons is set in order to reach a statistical uncertainty in dose at the isocenter lower or equal to 1% . Finally, the mean efficiency $\bar{\epsilon}_R$ for region R is calculated as follows:

$$\bar{\epsilon}_R = \frac{1}{N_{\mathrm{vox}}} \sum_{k=0}^{N_{\mathrm{vox}}} \epsilon_k \tag{7}$$

where N_{vox} is the number of voxels in region R.

4. Results

4.1. Impact of the kerma approximation

The comparison between dose distributions with electron production cuts of 10 μm and 1.0 m (kerma approximation) is shown in figure 2. For both dose distributions, the number of incident photons was set in order to achieve an average statistical uncertainty of 1% in the entire volume. We only show the mouse test case but similar results were obtained for the rat test case.

The dose difference map (left) shows an underestimation of dose in water and an overestimation in bone at the water/bone interfaces when using the kerma approximation. The average of the absolute value of the dose difference is about 2% of the prescribed dose at the isocenter when considering the entire volume, but can reach up to 12 to 14% in the highest dose regions. This dose delocalization from the water to the bone can easily be explained by the absence of electrons generated in bone at the water/bone interfaces. Indeed, the mean energy of electrons generated in the bone medium for the 225 kV incident spectrum is about 55 keV. Even if the corresponding mean free path is only a tenth of the voxel size (30 μm), the high number of electrons generated by the photoelectric effect in bone compared to water is sufficient to slightly change the deposited dose. No such difference can be observed at the interface between water and lung. As shown in the dose profiles (right), when using the kerma approximation, the dose appears sharper at the water/bone interfaces than with the full electron tracking method. We can also notice an aliasing effect when the distance to the isocenter

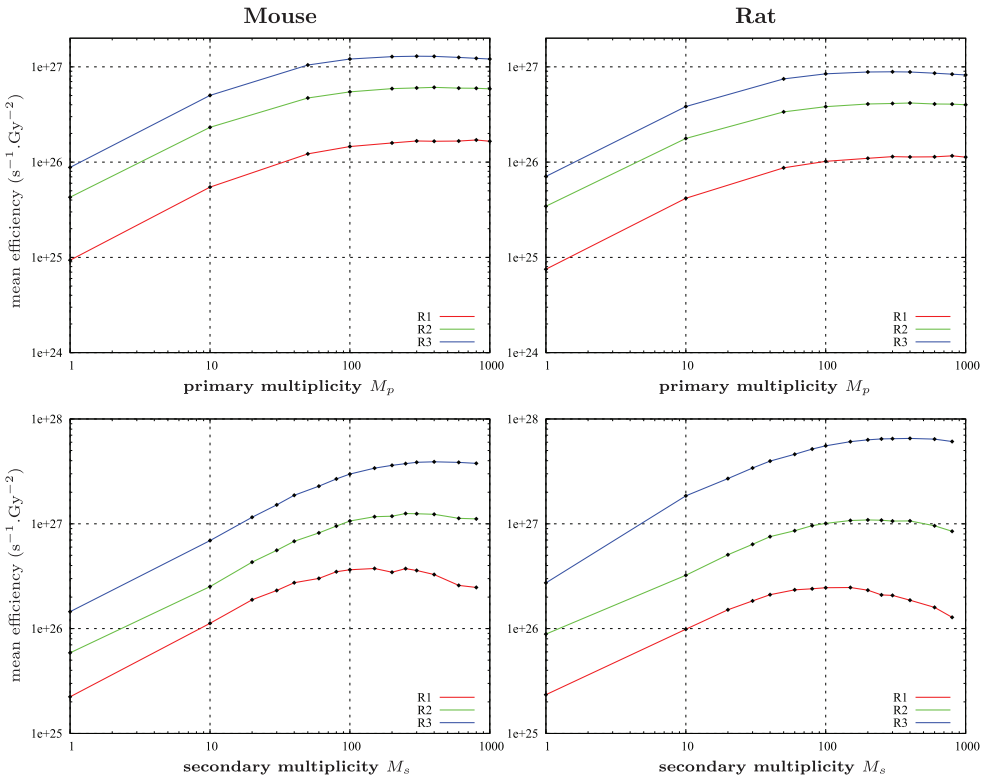

Figure 3. Mean efficiency as a function of the primary (top) and secondary (bottom) multiplicity in regions R_1, R_2 and R_3, for the mouse (left) and rat (right) test cases. The incident number of photons was set to 10^5 for each simulation point. Primary and secondary dose simulations were performed separately, i.e. $M_s = 0$ for the primary and $M_p = 0$ for the secondary.

increases (see figure 2). This artifact in the dose difference map is an interference between incident beams and is governed by the beam profile, the beam angular spacing and the incident energy spectrum (mean free path of electrons). This artifact disappears for beam angle spacing lower than two degrees. Finally, we can note that the influence of the kerma approximation on the dose distribution is the same for the MC, TLE and seTLE dose scoring methods.

4.2. seTLE optimal multiplicities

Figure 3 represents the mean efficiency in regions R_1, R_2 and R_3 for the mouse (left) and rat (right) test cases as a function of the primary (top) and secondary (bottom) splitting multiplicities.

We can see that each multiplicity curve is characterized by a fast increase of the efficiency for small multiplicity values and an optimum value. Beyond the optimum value, the efficiency stays rather constant for primary multiplicity curves and decreases for secondary multiplicity curves. We can also note that the primary optimal multiplicity seems rather independent of the region, contrary to the secondary optimal multiplicity which increases (from about 150 to 500) when the diameter of the region increases (from R_1 to R_3). Indeed, the secondary dose contribution results from the photon interaction sites which display the highest density at the

Table 1. Incident particle number, simulation time and dose uncertainty at the isocenter for analog MC, TLE and seTLE reference dose distributions.

	Mouse			Rat		
	N	t (min)	$\sigma_{iso}(\%)$	N	t (min)	σ_{iso} (%)
Analog MC	1×10^{10}	1.5×10^{5}	0.4	1×10^{10}	2.1×10^{5}	0.6
TLE	1×10^{7}	161	0.6	2×10^{7}	432	1.0
seTLE	1×10^{5}	32	0.4	2×10^{5}	101	0.6

Table 2. Integral and confidence interval (99%) of the dose deposited in the $(R_1 + R_2 + R_3)$ ROI, expressed in nGy per incident photon, for the analog MC, TLE and seTLE dose scoring methods.

	Mouse model	Rat model
AnalogMC	46.49 ± 0.01	92.10 ± 0.01
TLE	46.66 ± 0.02	92.30 ± 0.05
seTLE	46.70 ± 0.08	92.36 ± 0.10

isocenter. The probability for a voxel to be traversed by a hybridino is therefore naturally high close to the isocenter and, consequently, the R_1 region requires a lower multiplicity value. This also explains the difference of optimal secondary multiplicities in region R_1 between the mouse case ($M_s \approx 200$), mainly composed of water and rat case ($M_s \approx 100$), mainly composed of bone.

Despite the differences between test cases, regions and dose contributions, the primary and secondary optimal multiplicities can be fixed to a single value without any significant loss of efficiency. For both test cases, the primary and secondary multiplicity values, M_p and M_s, are set to 300. The worst efficiency loss is about 15% for region R_1 of the rat test case for the secondary dose contribution.

4.3. Dose and efficiency comparisons

Table 1 gathers the incident particle numbers used for simulating the dose distributions for the analog MC, TLE and seTLE methods, the corresponding simulation times and the final dose uncertainty at the isocenter. In practice, the analog MC, TLE and seTLE were respectively split into 100, 50 and 10 independent jobs which have been merged to obtain the final dose distributions. The simulation time corresponds to the expected time on a single CPU core.

The comparison of integral doses between analogMC, TLE and seTLE methods is presented in table 2. We can see that the TLE and seTLE dose values converge to the same results (within the confidence interval). The comparison between kerma-based methods and analog MC reveals a bias inferior to 0.5% . This bias may be due to the set of energy absorption coefficients generated using the EPDL97 database (Mittone *et al* 2013). Indeed, parameters of the MC simulation such as production cuts can slightly influence the energy deposits. In terms of local dose comparison, the 2D gamma index results with the analog MC as the reference show that 99.9% for TLE and 99.8% for seTLE of the voxels in the isocenter irradiation plane satisfy the 0.3 mm distance/1% of dose at the isocenter criterion.

The mean efficiencies for the three scoring methods are grouped in table 3. The comparison of kerma-based techniques to analog MC shows a gain in efficiency of about 4 orders

Table 3. Mean efficiency in regions R_1, R_2 and R_3 for the analog MC, TLE and seTLE dose scoring methods.

	Mouse model			Rat model		
ϵ ($s^{-1}.Gy^{-2}$)	R_1	R_2	R_3	R_1	R_2	R_3
Analog MC	4.74×10^{19}	2.95×10^{20}	2.74×10^{21}	7.47×10^{19}	5.71×10^{20}	3.41×10^{21}
TLE	2.74×10^{24}	1.53×10^{25}	3.81×10^{25}	1.94×10^{24}	1.68×10^{25}	1.11×10^{26}
seTLE	3.64×10^{25}	2.10×10^{26}	5.57×10^{26}	2.38×10^{25}	2.23×10^{26}	1.67×10^{27}
$\epsilon_{seTLE}/\epsilon_{TLE}$	13.3	13.7	14.6	12.3	13.3	15.0

of magnitude for the TLE method and of 5 orders of magnitude for the seTLE method. The comparison of the seTLE with the TLE method shows a global gain, varying from 13.3 to 14.6 for the mouse test case and from 12.3 to 15.0 for the rat test case. First, these variations can be explained by the choice of the optimal multiplicity values of 300 (section 4.2). Although this value was a good compromise for all regions and test cases, we reported a slight loss in efficiency for the secondary dose contribution as the region size decreases. Second, the mean material density in the region also influences the efficiency. In figure 4, we show the maps of the efficiency gain between the three methods. When comparing the TLE (A,B) or seTLE (C,D) with the analog MC method, we can see that the gain in efficiency depends on the material density, i.e. the lower the density, the higher the gain. However, we observe that the seTLE produces many low efficiency spots. The same phenomenon is visible in the comparison between the seTLE and TLE, where the spot concentration is higher in the high density regions (femoral head of the rat case) than in the low density regions (lung of the mouse case). These spots are a direct consequence of the exponential law of the seTLE which increases the dose uncertainty near production/scattering sites of photons (Smekens *et al* 2009).

5. Discussion

In this study, we have investigated the seTLE method based on a combination of MC splitting, hybrid ray casting/MC navigation and expTLE dose scoring. For both the TLE and seTLE methods, the difference in terms of integral dose is below 0.5% compared to analog MC and the 2D gamma index criterion (1% of the dose at the isocenter, 0.3 mm) is fulfilled. We showed that the seTLE technique accelerates dose simulation of typical small animal treatment plans 13 to 15 times compared to the state-of-the-art TLE method. The simulation time of the mouse plan to obtain a 1% dose uncertainty at the isocenter can be reduced from 66 to 5 minutes considering a single CPU core and a dose grid resolution of 0.2 mm.

The only approximation of the kerma-based techniques is the complete deactivation of electrons. The effect of this approximation is an overestimation/underestimation of dose in bone/water at the interface of the two materials. The average dose delocalization, expressed in percentage of the dose at the isocenter, is about 2% when considering the entire volume but can reach 14% where the dose is the highest. It should be noted that the selected test cases are very challenging for testing the kerma approximation since the isocenter is placed in highly heterogeneous regions. Moreover, the small number of materials (air, lung tissue, soft tissue, cortical bone, carbon) as well as the voxel size of $0.2 \times 0.2 \times 0.2$ mm^3 emphasize the electron disequilibrium. The validity of the kerma approximation generally depends on the balance between the mean incident x-ray energy and the volume resolution. Indeed, the electron disequilibrium increases with the incident beam energy and becomes more visible as the voxel size decreases. It is worthy of note that many low energy photon dosimetry applications at

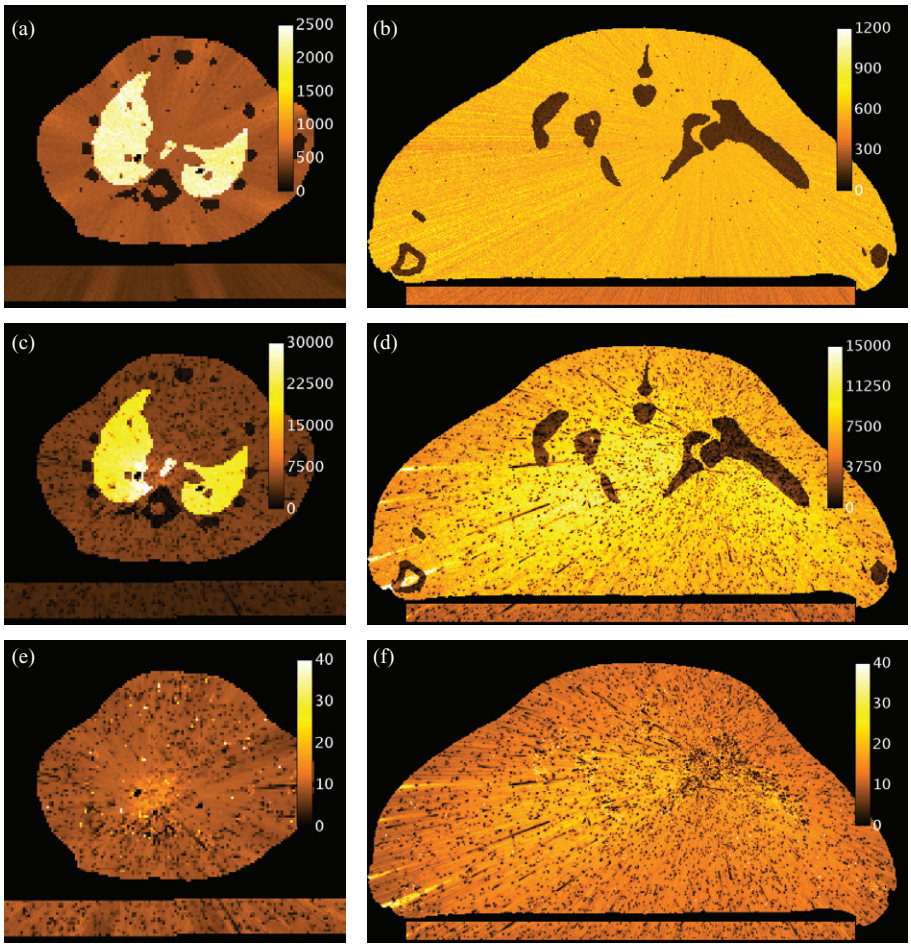

Figure 4. Efficiency gain maps $\epsilon_{\mathrm{TLE}}/\epsilon_{\mathrm{analogMC}}$ (*a*, *b*), $\epsilon_{\mathrm{seTLE}}/\epsilon_{\mathrm{analogMC}}$ (*c*, *d*) and $\epsilon_{\mathrm{seTLE}}/\epsilon_{\mathrm{TLE}}$ (*e*, *f*) for the mouse (*a*, *c*, *e*) and rat (*b*, *d*, *f*) test cases.

the human scale (brachytherapy, synchroton radiation therapy, radioprotection, CB-CT, etc.) present more favorable simulation conditions.

By using the splitting strategy, we introduced two new parameters: the primary and secondary splitting multiplicities M_{p} and M_{s}. The optimal multiplicity values depend on the irradiation setup (volume dimension and resolution, materials, incident beam, etc.). For typical small animal treatment plans, a single multiplicity of $M_{\mathrm{p}} = M_{\mathrm{s}} = 300$ seems a good compromise for the three spherical isocentric ROIs. However, the optimal multiplicity values will differ if the local dose contribution ratio changes (primary dose versus secondary dose).

The main asset of the seTLE method is the hybridino transportation engine which is free of any MC physics process. Indeed, the time to propagate a hybridino (and to calculate the associated dose) is about 50 to 100 times lower compared to the time to propagate a photon. This makes the hybridino splitting extremely efficient compared to MC photon splitting, where the real benefit is for situations where photon interactions are scarce. In our situation, the mean free path in water ranges from 1 to 7 cm for the considered incident x-ray spectrum. Therefore

for such a radiation therapy application, a MC photon splitting (that could be applied to both the conventional TLE and the seTLE methods incidentally) would not gain much in efficiency.

The TLE-based techniques require a set of energy absorption coefficients and attenuation coefficients (for expTLE and seTLE) for each material in the simulation. Although these data can be accessed from official databases, they consider a real physics environment which is generally not reproduced in the MC simulation (differences in MC models, cuts on particles, etc.). Hence, a tool designed to produce attenuation and energy absorption coefficients using the MC inputs would be highly valuable for the comparison of VRTs.

The classical VRTs (MC splitting or Russian roulette strategies) are generally used to improve the statistics of rare or time-consuming physical interactions (e.g. the bremsstrahlung effect for x-ray production). In the seTLE, the splitting is entirely dedicated to dose calculation with hybridinos and, therefore, does not impact the MC transportation of physical particles. As any existing kerma-based method, it is allowed to combine the seTLE with other VRTs. Indeed, the results presented in this work rely on simple management of the primary and secondary splitting multiplicities, i.e. a single multiplicity value for the entire volume. The use of additional VRTs, such as Russian roulette or importance sampling, could provide additional gain in efficiency.

6. Conclusion

In this study, we presented a new kerma-based dose scoring method, the seTLE (split exponential track length estimator), combining MC splitting, ray casting/MC navigation and exponential TLE dose scoring. We demonstrated that the seTLE is able to improve the MC efficiency of typical small animal treatment plans by one order of magnitude compared to the state-of-the-art TLE dose scoring. Additionally, we explored and discussed the validity of the kerma approximation for such applications.

Acknowledgments

This work was performed in part within the LABEX PRIMES (ANR-11-LABX-0063/ANR-11-IDEX-0007) of Université de Lyon operated by the French National Research Agency, and partly supported by Lyric INCa-DGOS-4664, MC SMART (AVIESAN, INCa) and t-Gate (ANR-14-CE23-0008).

References

Baldacci F *et al* 2014 A track length estimator method for dose calculations in low-energy x-ray irradiations: implementation, properties and performances *Z. Med. Phys.* (doi:10.1016/j.zemedi.2014.04.001)

Bazalova M, Zhou H, Keall P J and Graves E E 2009 Kilovoltage beam Monte Carlo dose calculations in submillimeter voxels for small animal radiotherapy *Med. Phys.* **36** 4991–9

Brualla L, Salvat F and Palanco-Zamora R 2009 Efficient Monte Carlo simulation of multileaf collimators using geometry-related variance-reduction techniques *Phys. Med. Biol.* **54** 4131–49

Chetty I J, Rosu M, Kessler M L, Fraass B A, Haken R K T, Kong F M and McShan D L 2006 Reporting and analyzing statistical uncertainties in Monte Carlo-based treatment planning *Int. J. Radiat. Oncol. Biol. Phys.* **65** 1249–59

Clarkson R, Lindsay P E, Ansell S, Wilson G, Jelveh S, Hill R P and Jaffray D A 2011 Characterization of image quality and image-guidance performance of a preclinical microirradiator *Med. Phys.* **38** 845–56

Freud N, Létang J M, Mary C, Boudou C, Ferrero C, Elleaume H, Bravin A, Estève F and Babot D 2008 A hybrid approach for fast simulation of dose deposition in stereotactic synchrotron radiotherapy *IEEE Trans. Nucl. Sci.* **55** 1008–17

Granton P V and Verhaegen F 2013 On the use of analytic source model for dose calculations in precision image-guided small animal radiotherapy *Phys. Med. Biol.* **58** 3377–95

Grevillot L, Frisson T, Maneval D, Zahra N, Badel J N and Sarrut D 2011 Simulation of 6 MV elekta precise linac photon beam using GATE/GEANT4 *Phys. Med. Biol.* **56** 903–18

Jan S *et al* 2011 GATE V6 : a major enhancement of the GATE simulation platform enabling modelling of CT and radiotherapy *Phys. Med. Biol.* **56** 881–901

Kawrakow I and Fippel M 2000 Investigation of variance reduction techniques for Monte Carlo photon dose calculation using XVMC *Phys. Med. Biol.* **45** 2163–83

Mainegra-Hing E and Kawrakow I 2006 Efficient x-ray tube simulations *Med. Phys.* **33** 2683–90

Mittone A *et al* 2013 An efficient numerical tool for dose deposition prediction applied to synchrotron medical imaging and radiation therapy *J. Synchrotron Radiat.* **20** 785–92

Poludniowski G, Landry G, DeBlois F, Evans P M and Verhaegen F 2009 SpekCalc: a program to calculate photon spectra from tungsten anode x-ray tubes *Phys. Med. Biol.* **54** N433

Rodriguez M, Sempau J and Brualla L 2012 A combined approach of variance-reduction techniques for the efficient Monte Carlo simulation of linacs *Phys. Med. Biol.* **57** 3013–24

Sarrut D *et al* 2014 A review of the use and potential of the GATE Monte Carlo simulation code for radiation therapy and dosimetry applications *Med. Phys.* **41** 064301

Smekens F, Freud N, Létang J M, Adam J F, Ferrero C, Elleaume H, Bravin A, Estève F and Babot D 2009 Simulation of dose deposition in stereotactic synchrotron radiation therapy: a fast approach combining Monte Carlo and deterministic algorithms *Phys. Med. Biol.* **54** 4671–85

Verhaegen F, Granton P and Tryggestad E 2011 Small animal radiotherapy research platforms *Phys. Med. Biol.* **56** R55–83

Williamson J F 1987 Monte Carlo evaluation of kerma at a point for photon transport problems *Med. Phys.* **14** 567–76